BIOCHEMISTRY
including biophysical chemistry & molecular biology

Article

pubs.acs.org/biochemistry

Spectroscopic and Kinetic Investigation of the Reactions of Peroxyacetic Acid with *Burkholderia pseudomallei* Catalase-Peroxidase, KatG

Anabella Ivancich,[†] Lynda J. Donald,[‡] Jacylyn Villanueva,[‡] Ben Wiseman,[‡] Ignacio Fita,[§] and Peter C. Loewen*[,‡]

[†]CNRS, Unité de Recherche Mixte CNRS/CEA/Université Paris Sud (UMR 8221), Laboratoire de Bioénergétique, Métalloprotéines et Stress, Centre d'Etudes de Saclay/iBiTec-S, 91191 Gif-sur-Yvette, France

[‡]Department of Microbiology, University of Manitoba, Winnipeg, Manitoba R3T 2N2, Canada

[§]Institut de Biología Molecular de Barcelona (CSIC) and IRB Barcelona, Parc Científic de Barcelona, Baldiri i Reixac 10-12, 08028 Barcelona, Spain

ABSTRACT: Catalase-peroxidases or KatGs can utilize organic peroxyacids and peroxides instead of hydrogen peroxide to generate the high-valent ferryl-oxo intermediates involved in the catalase and peroxidase reactions. In the absence of peroxidatic one-electron donors, the ferryl intermediates generated with a low excess (10-fold) of peroxyacetic acid (PAA) slowly decay to the ferric resting state after several minutes, a reaction that is demonstrated in this work by both stopped-flow UV−vis absorption measurements and EPR spectroscopic characterization of *Burkholderia pseudomallei* KatG (*Bp*KatG). EPR spectroscopy showed that the [Fe^{IV}=O $Trp_{330}^{\bullet+}$], [Fe^{IV}=O $Trp_{139}^{\bullet}$], and [Fe^{IV}=O $Trp_{153}^{\bullet}$] intermediates of the peroxidase-like cycle of *Bp*KatG (Colin, J., Wiseman, B., Switala, J., Loewen, P. C., Ivancich, A. (2009) *J. Am. Chem. Soc. 131*, 8557−8563), formed with a low excess of PAA at low temperature, are also generated with a high excess (1000-fold) of PAA at room temperature. However, under high excess conditions, there is a rapid conversion to a persistent [Fe^{IV}=O] intermediate. Analysis of tryptic peptides of *Bp*KatG by mass spectrometry before and after treatment with PAA showed that specific tryptophan (including W_{330}, W_{139}, and W_{153}), methionine (including Met_{264} of the M−Y−W adduct), and cysteine residues are either modified with one, two, or three oxygen atoms or could not be identified in the spectrum because of other undetermined modifications. It was concluded that these oxidized residues were the source of electrons used to reduce the excess of PAA to acetic acid and return the enzyme to the ferric state. Treatment of *Bp*KatG with PAA also caused a loss of catalase activity towards certain substrates, consistent with oxidative disruption of the M−Y−W adduct, and a loss of peroxidase activity, consistent with accumulation of the [Fe^{IV}=O] intermediate and the oxidative modification of the W_{330}, W_{139}, and W_{153}. PAA, but not H_2O_2 or *tert*-butyl hydroperoxide, also caused subunit cross-linking.

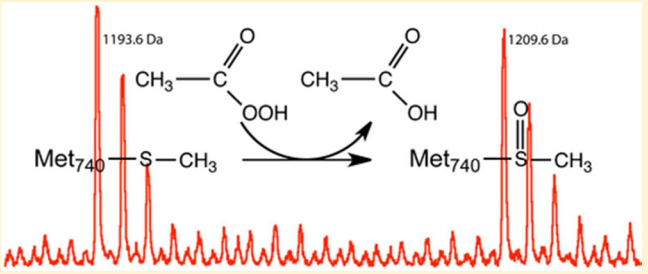

Catalases and peroxidases have evolved to remove hydrogen peroxide and thereby prevent cellular damage caused by its more reactive breakdown products. Catalases, whether dimanganese- or heme-containing, catalyze the dismutation of hydrogen peroxide ($2H_2O_2 \rightarrow 2H_2O + O_2$) in a two-step process. In heme-containing catalases, one H_2O_2 heme in its resting (ferric, Fe^{III}) oxidation state to the compound I intermediate, the [Fe^{IV}=O $Por^{\bullet+}$], which is subsequently reduced back to the resting state by a second H_2O_2. The peroxidase reaction ($H_2O_2 + 2A + 2H^+ \rightarrow 2H_2O + 2A^{\bullet+}$) is also a two-step process but with organic or metal ion electron donors (A) acting as one-electron reductants of the [Fe^{IV}=O $Por^{\bullet+}$] intermediate.[1]

Catalase-peroxidases or KatGs are unique in catalyzing both reactions albeit with the catalatic reaction being significantly faster ($k_{cat} \approx 9 \times 10^3$ s^{-1}) than the peroxidatic reaction ($k_{cat} \approx 20$ s^{-1}).[2] In fact, these rates are considerably slower than those of the monofunctional enzymes such as *Proteus mirabilis* catalase ($k_{cat} = 8.3 \times 10^5$ s^{-1})[3] and horseradish peroxidase ($k_{cat} \approx 6 \times 10^3$ s^{-1}),[4] suggesting that the heme active site of KatGs has evolved as a compromise that accommodates the two reactions but is not optimized for either. The KatG-unique M−Y−W cross-linked structure and associated mobile arginine is a structural adaptation of the peroxidase core that is essential for catalatic activity (Figure 1).[5] Compromise is further evident in the functional versatility of KatGs, which support isonicotinyl-NAD synthesis (pro-drug INH activation), INH cleavage, NADH oxidation, and superoxide generation, albeit all at much slower rates (0.002−0.5 s^{-1}).[6−8]

Received: July 18, 2013
Revised: September 16, 2013
Published: September 17, 2013

   dx.doi.org/10.1021/bi400963j | *Biochemistry* 2013, 52, 7271−7282

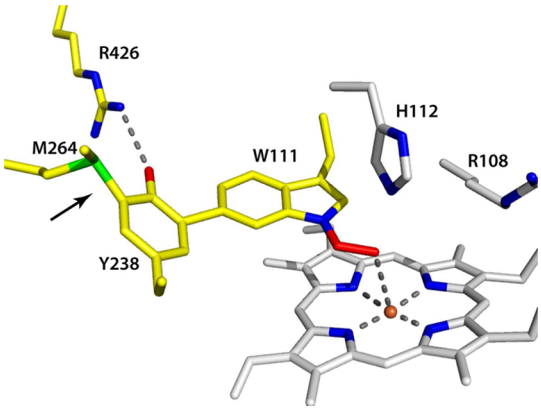

Figure 1. View of the distal side of the active site heme cavity of *Burkholderia pseudomallei* KatG at pH 7.5. The heme and the catalytic residues, Arg108 and His112, are shown in gray. The M−Y−W adduct and mobile Arg426 required for catalatic activity are shown in yellow. The perhydroxy modification on W_{111}−OOH in one of its two conformers associated with the heme iron is shown in red. The arrow indicates the site of adduct cleavage discussed in the text. The figure was prepared by using the coordinates deposited in the Protein Data Bank (accession no. 2B2Q).

In the presence of low concentrations of H_2O_2[9−11] or alternate oxidants such as PAA[11−13] and *t*BHP,[9,11,13−16] but in the absence of peroxidatic substrates, KatGs are oxidized to a short-lived [Fe^{IV}=O $Por^{\bullet+}$] intermediate and relatively stable [Fe^{IV}=O $Trp^{\bullet}$] intermediates.[11,13] In heme monofunctional peroxidases, substrates bind close to the heme δ and γ edges (reviewed in ref 17) allowing for facile electron transfer directly to the oxidized heme or in other cases may bind at sites remote from the heme requiring electron transfer through the protein to the heme.[18] The only peroxidatic ligand-binding site so far characterized on KatGs is that of INH, which is found far from the heme in *Bp*KatG,[6] and its oxidation involves electron transfer to the oxidized heme via a tryptophan-based radical intermediate.[19] The binding sites of the more commonly used peroxidatic substrates, ABTS and *o*-dianisidine, have not yet been identified in KatGs although the evidence that the latter can inhibit the catalatic reaction[20] suggests that it may bind close to the heme.

While our understanding of some aspects of the KatG catalytic mechanisms has improved with the identification of the unusual structural features of the heme site and the electronic nature of the intermediates, some of the questions that remain open are the focus of this report. In particular, a phenomenon that lacks a satisfactory explanation is the slow reduction to the resting state of PAA-generated high-valent intermediates in the absence of exogenous electron donor(s).[21] A similar reaction involving the reduction of high-valent ferryl-oxo intermediates of the chloroperoxidase from *Caldariomyces fumago* to the ferric state utilizing electrons drawn from *m*CPBA has been reported,[22] although PAA did not support the same chemistry in this instance. A related phenomenon, also without a clear explanation, is the reported oxidatively induced dimerization of *Mycobacterium tuberculosis* KatG (*Mt*KatG) and apparent progressive conversion to larger oligomers.[16]

In this report, we present evidence that the reaction of *Bp*KatG with high levels of PAA and in the absence of exogenous electron donors results in the oxidative modification of specific tryptophan, methionine, and cysteine residues. In particular, the internal oxidation of Met_{264} and resulting disruption of the M_{264}−Y_{248}−W_{111} adduct can be linked to the PAA-induced loss of catalatic activity, while the loss of peroxidatic activity and accumulation of a [Fe^{IV}=O] intermediate can be correlated with the modification of W_{330}, W_{139}, and W_{153} sites of protein-based radical intermediates formed in the peroxidase-like reaction of *Bp*KatG.

EXPERIMENTAL PROCEDURES

Enzyme Preparation and Assays. *Bp*KatG and *Mt*KatG were expressed in *Escherichia coli* strain UM262 *pro leu rpsL hsdM hsdR endI lacY katG17::Tn10 katE1 recA*[23] and purified as described previously.[24,25] Catalase activity was determined by the method of Rørth and Jensen[26] in a Gilson oxygraph equipped with a Clark electrode. One unit of catalase is defined as the amount that decomposes 1 μmol of H_2O_2 in 1 min in a 60 μM H_2O_2 solution at pH 7.0 and 37 °C. Peroxidase activity was determined using ABTS (ε_{405} = 36 800 M^{-1} cm^{-1})[27] as electron donor. PAA, *m*CPBA, and *t*BHP were diluted in an appropriate buffer to a concentration 100-fold higher than was used in individual experiments and treated with 0.1 mg/mL bovine liver catalase for 10 min at 20 °C prior to use. One unit of peroxidase is defined as the amount that decomposes 1 μmol of ABTS in 1 min in a solution of 0.4 mM ABTS at pH 5.0 and 25 °C. In the standard assay, 2.5 mM H_2O_2 is used, but other oxidants were employed as noted. Protein was estimated according to the method of Layne.[28] Where noted, 3 μg/mL glucose oxidase and 5 mM glucose were used to generate low levels (7 μM/min[4]) of H_2O_2. Gel electrophoresis of purified proteins was carried out under denaturing conditions on 8% SDS-polyacrylamide gels.[29,30] Samples were treated as described in the figure legend prior to electrophoresis.

Stopped-Flow UV−vis Absorption Measurements. Time-dependent UV−vis absorption spectra were obtained using a four-syringe SX20 stopped-flow spectrophotometer (Applied PhotoPhysics Ltd.) equipped for conventional and sequential stopped-flow measurements with an attached diode array detector. A refrigerating bath (Huber Minichiller) was used to regulate the temperature of the samples in the syringes and in the mixing cell to 10 °C. All measurements were performed using an optical cell with a path length of 5 cm, and the shortest time for mixing and recording the first data point was 6.4 ms. The enzyme samples were at an initial concentration of 170 μM and mixed with an equal volume of 15-folds excess PAA at pH 7.0 (in 50 mM Tris-maleate buffer). Data were recorded using 500 data points on a logarithmic scale and over a total time of 15 min. The wavelengths quoted in the text and figures for the heme charge-transfer bands were determined at the full-width half-maximum (FWHM).

EPR Spectroscopy and Sample Preparation. The 9 GHz EPR spectra were recorded on a Bruker EleXsys E500 spectrometer equipped with a standard Bruker ER 4102 X-band resonator and a liquid helium cryostat (Oxford Instruments, ESR 900). EPR quartz tubes of 4 mm external diameter were used. The EPR sample used to monitor the complete reaction of *Bp*KatG with low excess (10-fold) of PAA and to compare with the stopped-flow experiments was prepared by manual mixing of 40 μL of native *Bp*KatG (initial concentration of 0.8 mM, at pH 6.4 in 50 mM Tris-maleate buffer) with an equal volume of 10-fold excess PAA (initial concentration of 8 mM at pH 6.4 in 50 mM Tris-maleate buffer). The mixing was done on ice for 10 s followed by flash freezing in liquid nitrogen. The same sample (80 μL) was thawed and immediately diluted in 2

dx.doi.org/10.1021/bi400963j | *Biochemistry* 2013, 52, 7271−7282

mL of 50 mM Tris-maleate, pH 8.0 (to avoid precipitation due to acidification induced by the acetic acid product generated in the enzyme reaction with PAA). Recycling of the enzyme to the ferric oxidation state was achieved by resuspending and concentrating three times using 2 mL of buffer in a Centricon microconcentrator (Amicon). Tris-maleate buffer at pH 6.5 was used in the last wash to adjust the pH of ferric *Bp*KatG.

EPR samples used to compare the reaction with low and high excesses of PAA were prepared by mixing manually 40 μL of native *Bp*KatG in 50 mM Tris-maleate buffer, pH 6.4 (initial concentration of 0.4 mM), with an equal volume of 10-fold or 1000-fold excesses of buffered PAA (pH 5.0) for 4 or 2 s, respectively, and flash frozen in liquid nitrogen. The mixing was done in the 4 mm-EPR tubes at 20 °C. The low-temperature intramolecular electron transfer between intermediates was monitored by incubating the PAA-reacted *Bp*KatG samples in a methanol/CO_2 bath (−80 °C) for 15 min. After thawing in ice, the PAA-reacted *Bp*KatG samples were incubated for further 20 min to monitor the changes of the EPR spectrum upon reaction with PAA over a longer period of time.

Mass Spectrometry Analysis. *Bp*KatG at 12 μM in 50 mM NH_4HCO_3 was treated with 0.1, 1, and 10 mM PAA (10-, 100-, and 1000-fold excesses, respectively) for 15 min at 20 °C, transferred to ice, and then washed 4 times with 50 mM NH_4HCO_3 in an Ultrafree 30K spin filter. The protein was redissolved in 50 μL of NH_4HCO_3, mixed with 5 μL of 0.01 mg/mL trypsin, and incubated at 37 °C for 16 h. The digested samples were mixed with an equal volume of matrix (2,5-dihydroxybenzoic acid) and deposited on a metal plate that fits into a MALDI QqTOF mass spectrometer.[31,32] Spectra were acquired and analyzed using software developed in the time-of-flight laboratory in the Department of Physics and Astronomy, University of Manitoba, Canada. Ions selected for tandem mass spectra were analyzed by visual comparison of the ions expected from the known sequence to those observed in the spectrum. Protein samples before and after PAA treatment were also analyzed by electrospray ionization mass spectrometry [33] prior to trypsin digestion.

RESULTS

The spontaneous conversion of high-valent ferryl-oxo intermediates of *Synechocystis* KatG to the ferric resting state after reaction with PAA and in the absence of an added electron donor has been noted previously[21] but never fully documented. We have investigated this phenomenon further by using a combination of stopped-flow UV−vis electronic absorption spectroscopy, EPR spectroscopy, mass spectrometry, and activity measurements on *Bp*KatG reacted with low (10- or 15-fold) and high (1000-fold) excesses of PAA.

Reaction of *Bp*KatG with Low Excess of PAA Monitored by Stopped-Flow UV−vis Absorption Spectrophotometry and EPR Spectroscopy. The changes in the 450−800 nm region of the electronic absorption spectrum of *Bp*KatG at pH 7.0 upon reaction with a 15-fold excess PAA and as a function of time up to 12 min are shown in Figure 2. This spectral region contains the heme charge-transfer (CT) bands, which are highly informative about changes in the iron oxidation state. A high enzyme concentration was chosen for this experiment in order to obtain well-resolved spectra in this region, despite the signal saturation in the heme Soret-band spectral region. The changes in the spectra following PAA addition perfectly match those previously reported in the full range spectrum recorded with lower enzyme concentrations

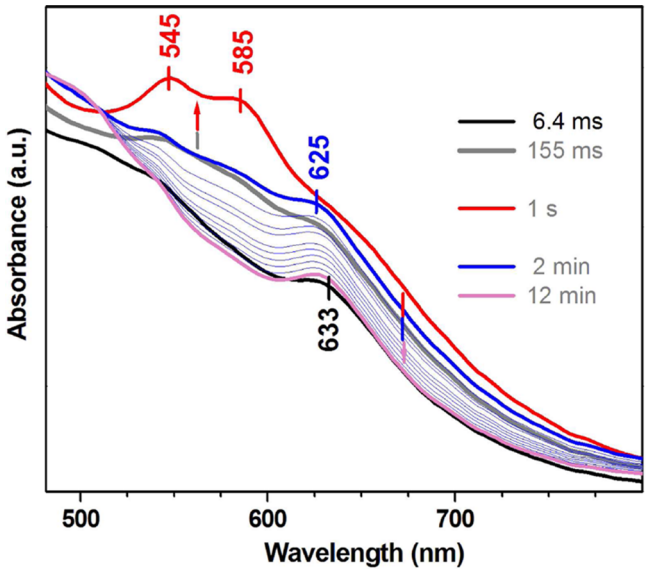

Figure 2. Rapid-scan electronic absorption spectra of the reaction of wild-type *Bp*KatG at pH 7.0 with a 15-fold excess of PAA. Selected spectra representing the resting (ferric) enzyme (black trace), the Fe^{III}−PAA complex (thick gray trace), the ferryl-like intermediate (red trace), and the slow conversion (blue traces) to the initial ferric state (magenta trace) are shown. The transitional spectra in the millisecond time range, between 155 ms and 1 s, are not shown for clarity but illustrated by the bicolor gray−red arrow. Similarly, the red−blue−magenta arrow illustrates the transition from the ferryl-like intermediate to the final ferric enzyme. Experimental conditions: 10 °C, reaction temperature; 85 μM *Bp*KatG and 1.275 mM PAA, (final) concentrations. Data were recorded on a logarithmic time scale over a total period of 12 min.

typically used in stopped-flow experiments (see Figure 1 in ref 13). The heme band at 635 nm, characteristic of the high-spin ferric oxidation state of *Bp*KatG (Figure 2, thick black trace) shifts to 625 nm upon mixing with PAA (thick gray trace) within 155 ms, a result of the formation of the Fe^{III}−PAA complex as previously reported. [13] The features of a ferryl-like spectrum (CT bands at 545 and 585 nm) were partially observed as early as 300 ms, and a distinct spectrum with such predominant features was observed at 1 s (thick red trace). Finally, the transition of the ferryl-like *Bp*KatG spectrum back to the ferric spectrum was much slower (blue traces) with a distinct spectrum resolved at 2 min (thick blue trace) and completed at 12 min (thick magenta trace). It is noteworthy that the first spectrum resolved coincident with PAA depletion is that of the Fe^{III}−PAA complex with a CT band at 625 nm (thick blue trace for 2 min), which then reverts to the initial ferric enzyme spectrum with the CT band at 635 nm (thick magenta trace at 12 min). This CT band shift is explained by the reorganization of the distal side H-bonding network that occurs upon final depletion of PAA and is consistent with the model of two binding events or two binding sites for PAA. [13] Specifically, the sequence of intermediates reflected by the two distinct ferric-like spectra (Figure 2, blue and magenta traces) observed during the depletion of PAA was reversed compared with the initial reaction (Figure 2, black and gray traces), thus reflecting the slow exchange of the bound molecule of one nonreactive PAA (or acetic acid product) in the second binding site (see Figure 6 in ref 13).

Similarly, the reaction of *Bp*KatG with a 10-fold excess of PAA was monitored by EPR spectroscopy (Figure 3). As

dx.doi.org/10.1021/bi400963j | *Biochemistry* 2013, 52, 7271−7282

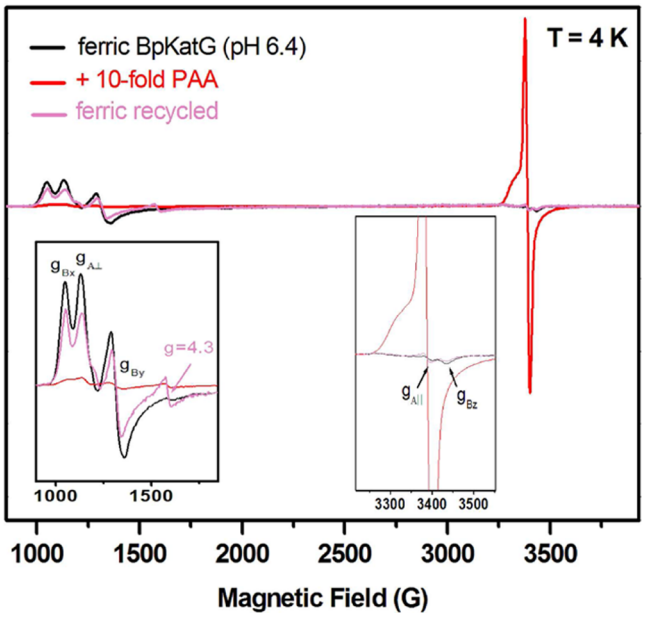

Figure 3. EPR spectra (9 GHz) of ferric *Bp*KatG (black trace) and upon reaction with a 10-fold excess of PAA at room temperature (red trace). The spectrum of the recovered ferric *Bp*KatG (magenta trace) is also shown. The insets show enlargements of the $g \approx 6$ and $g \approx 2$ components of the spectrum. Experimental conditions: temperature, 4 K; modulation amplitude, 4 G; microwave power, 1 mW; modulation frequency, 100 kHz; microwave frequency, 9.478 GHz.

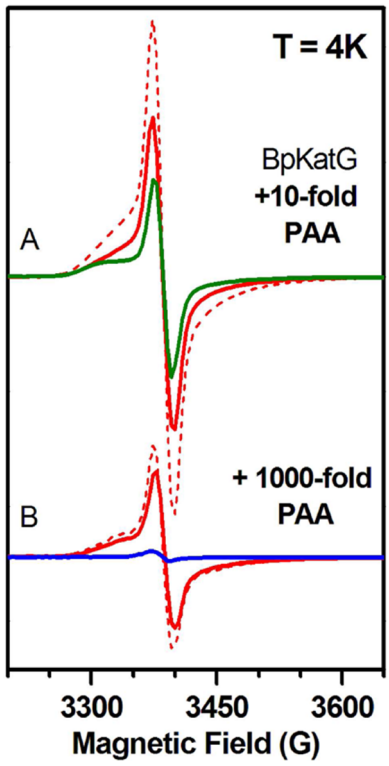

Figure 4. Comparisons of the 9-GHz EPR spectra, recorded at 4 K, of *Bp*KatG upon reaction (on ice) with a 10-fold excess of PAA and 4 s mixing time (A, solid red trace) and 1000-fold excess PAA and 2 s mixing time (B, solid red trace). EPR was also used to monitor intramolecular electron transfer between the intermediates in frozen solution, and by further incubation of the same two samples during 20 min at −80 °C (A, B, dotted red traces). The EPR spectra obtained after thawing and further incubating the same samples on ice for 20 min are also shown (A, green trace and B, blue trace). Experimental conditions: temperature, 4 K; modulation amplitude, 4 G; microwave power, 1 mW; modulation frequency, 100 kHz.

previously demonstrated,[34] the EPR spectrum of native *Bp*KatG is characteristic of a high-spin ($S = 5/2$) penta-coordinated ferric heme enzyme with two main resonances at $g \approx 6$ and $g \approx 2$ (Figure 3, black trace). The relative contribution of the axial (with $g_{A\perp} = 5.90$ and $g_{A\parallel} = 1.99$) and rhombically distorted (with $g_{Bx} = 6.50$, $g_{By} = 5.10$, and $g_{Bz} = 1.97$) signals to the EPR spectrum is pH-dependent (Figure 5 in ref 34). Upon reaction of *Bp*KatG with a 10-fold excess of PAA (Figure 3, red trace), the ferric EPR signals almost disappear (indicating a 90% conversion), accompanied with the concomitant formation of a broad EPR signal at $g \approx 2$, previously assigned to the high-valent ferryl-oxo intermediates of the reaction.[11] Specifically, the broad signal corresponds to the exchange-coupled $Trp_{330}^{\bullet+}$ of the $[Fe^{IV}{=}O\ W_{330}^{\bullet+}]$ species (Figure 3, red trace), with the contribution of a narrower EPR signal assigned to $Trp_{139}^{\bullet}$, $Trp_{153}^{\bullet}$, and a $Tyr^{\bullet}$.[11] Thawing and further incubation of the sample at room temperature for 30 min induced the disappearance of all protein-based radical EPR signals with no concomitant increase of the initial ferric heme signal (Figure 3, magenta trace), indicating conversion to a persistent EPR silent species, presumably the $[Fe^{IV}{=}O]$ intermediate. Yet, up to 70% of the initial ferric EPR signal, as estimated by comparison of the intensities of the EPR spectra (Figure 3, black and magenta traces), could be recovered (Figure 3, magenta trace) by washing the reacted sample several times against buffer (see Experimental Procedures). The absorption spectrum of the recycled sample was identical to that observed in the stopped-flow experiment after 12 min when the PAA had been depleted (see above). Moreover, the EPR spectrum of the recovered enzyme (magenta trace) was virtually identical to the initial spectrum (black trace), except for the appearance of a minor contribution of the signal with $g = 4.3$ of free iron, the latter consistent with the missing intensity of the ferric signal (see above). Accordingly, the recycled enzyme not only showed the same high-spin ferric EPR spectrum as the starting enzyme but also yielded the same protein-based radical intermediates (type and yields) upon reaction with PAA. Considering that the signal intensity of the recovered ferric heme and the yield of protein-based radical intermediates formed in a subsequent reaction with 10-fold excess PAA were both 30% lower than those of the initial enzyme, it was concluded that 70% of the enzyme was intact and fully active after recycling from reaction with a 10-fold excess of PAA.

Intermediates Formed during the Reaction of *Bp*KatG with a High Excess of PAA Monitored by EPR Spectroscopy. The intermediates and radical species formed using a very high excess (1000-fold) of PAA and room temperature, similar conditions to those used in the MS experiments described below, have been identified by EPR. Figure 4 shows the comparison of the 9-GHz EPR spectra of *Bp*KatG after reaction with a 10-fold excess (Figure 4A, red solid trace) and a 1000-fold excess (Figure 4B, red solid trace) of PAA, for 4 and 2 s, respectively, at room temperature. The EPR spectrum of the 1000-fold excess reaction shows that the same protein-based radical intermediates obtained by mixing with 10-fold excess PAA on ice (Figure 3) were formed, albeit with different relative yields of the three tryptophan-based radical species arising from temperature effects on the intramolecular electron-transfer events giving rise to the intermediates.

dx.doi.org/10.1021/bi400963j | *Biochemistry* 2013, 52, 7271−7282

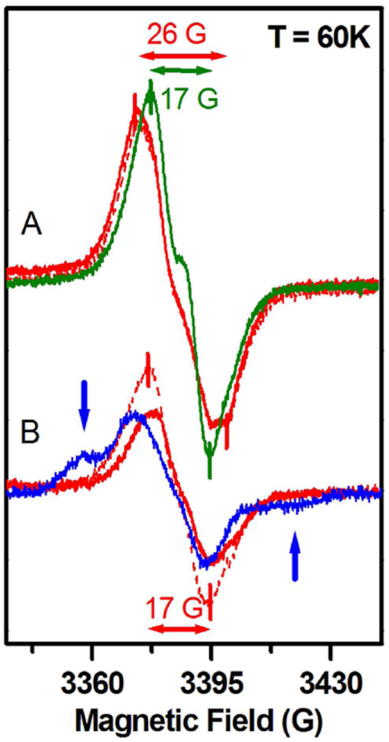

Figure 5. Comparison of the 9-GHz EPR spectra, recorded at 60 K, on the samples described in Figure 4. Experimental conditions: temperature, 60 K; modulation amplitude, 1.5 G; microwave power, 0.05 mW; modulation frequency, 100 kHz.

As we have previously demonstrated,[11] the broad EPR signal in the $g \approx 2$ spectral region with an overall width of 400 G (Figure 4A, red solid trace) is that of the exchange-coupled $Trp_{330}^{\bullet+}$ species (detected only with $T \leq 25$ K) and the narrower signal with a peak-to-trough width of 26 G better resolved at 60 K (Figure 5A, red solid trace) arises from the contributions of $Trp_{139}^{\bullet}$ and $Trp_{153}^{\bullet}$, plus a $Tyr^{\bullet}$ species (peak-to-trough width of 17 G in Figure 5A, green solid trace). When the same initial enzyme concentration and sample volume are used in the EPR tubes, it is possible to compare accurately the yield of the different radicals contributing to the spectra of *Bp*KatG upon reaction with low and high excesses of PAA. Accordingly, a comparison of the intensities of the EPR signals at 4 K (on the broad shoulders) shows that the yield of the [Fe^{IV}═O $W_{330}^{\bullet+}$] intermediate observed upon reaction with 1000-fold excess PAA (Figure 4B, red solid trace) is half of that obtained with a 10-fold excess of PAA (Figure 4A, red solid trace). Similarly, the EPR spectra recorded at 60 K (Figure 5) showed that the yields of radicals obtained with a 1000-fold excess of PAA (Figure 5B, solid red trace) are half those with the 10-fold excess (Figure 5A, solid red trace) and also that the relative contribution of the tyrosyl radical to the initial EPR spectrum is higher in the 1000-fold excess sample (Figure 5B, solid red trace). In summary, the same protein-based radical intermediates are formed with both low and high PAA excesses in 4 s and 2 s mixing times, respectively, but the reaction is accelerated with a 1000-fold excess of PAA, and the equilibrium among the intermediates shifts rapidly toward a predominant [Fe^{IV}═O] EPR-silent species.

Thawing and incubation of both samples on ice for 20 min, to allow the reaction with PAA to proceed further, resulted in a dramatic decrease of all three tryptophan radical signals (Figure 4A, green trace, and Figure 4B, blue trace) in both cases, indicating the conversion to a [Fe^{IV}═O] intermediate. A crucial difference is evident in the 60 K EPR spectra; the spectrum from a 10-fold excess of PAA showed only the $Tyr^{\bullet}$ signal (Figure 5A, green trace), whereas the spectrum from the 1000-fold excess of PAA showed a different radical signal (Figure 5B, blue trace). Unfortunately, the low yield of the new radical signal precluded a proper characterization of *g*-values using high-field EPR, but the temperature relaxation behavior and shoulders (blue arrows in Figure 5B) could be consistent with a sulfur-based radical in proximity to the heme iron, a possibility to be considered in the context of the MS results described below.

Intramolecular electron transfer among the tryptophan-based radical intermediates in frozen solution was also investigated by monitoring changes in the EPR spectra after incubation of the samples obtained with 10-fold and 1000-fold excesses of PAA (Figure 4A,B, red solid traces) for 20 min at −80 °C (Figure 4A,B, red dotted traces). Interestingly, the mixture with a 10-fold excess of PAA shows a 1.5 times increase of the exchange-coupled $Trp_{330}^{\bullet+}$ signal (Figure 4A, red dotted trace) but no change in the other radical signals in the 60 K EPR spectrum (Figure 5A, red dotted trace). In contrast, the 1000-fold excess sample shows a small increase (1.1 times) in the $Trp_{330}^{\bullet+}$ signal (Figure 5A, red dotted trace) but a 1.5 times increase in the 60 K EPR signal (Figure 4B, red dotted trace). These results clearly show that while intramolecular electron transfer between the catalytic protein-based radical intermediates occurs in a frozen solution at −80 °C, the formation of a radical tentatively assigned to a sulfur-based radical species only happens in solution at room temperature and in the presence of a very high excess of PAA.

PAA-Mediated Oxidative Modification of *Bp*KatG as Monitored by Mass Spectrometry. The process by which *Bp*KatG reduces an excess of PAA and itself is returned to the resting ferric state requires a source of electrons. For PAA to serve as both an oxidant and reductant like H_2O_2 does in catalases and *m*CPBA does for the *Caldariomyces fumago* chloroperoxidase,[22] molecular oxygen would be an expected product, yet none is detected during the reaction of *Bp*KatG with PAA (data not shown). Therefore, it was concluded that, in the absence of exogenous electron donors, *Bp*KatG itself must be the source of the electrons required for the reduction of PAA. Electrons from the formation of protein-based radicals in the peroxidatic cycle[11] are one obvious source, but additional tryptophans, methionines, and cysteines would be required to supply sufficient electrons to react with larger excesses of PAA. Surface situated methionine and cysteine residues may undergo direct oxidation by PAA to produce sulfur oxide species, whereas indole and internal sulfur-based radicals arising from electron transfer to the ferryl heme species in the peroxidatic cycle may, in the absence of a peroxidatic substrate, react with water or oxygen to produce indole oxide and sulfur oxide species. The oxidative modification of residues in PAA-treated *Bp*KatG was investigated in a mass spectrometry analysis of tryptic peptides before and after treatment with 0-, 10-, 100-, and 1000-fold excess PAA.

Generally, increasing amounts of PAA resulted in increasing amounts of oxidation, but only the results from a 15 min, 1000-fold excess treatment are presented because they best illustrate the extent of oxidation (Table 1). Two classes of changes in a significant number of tryptophan-, methionine-, and cyteine-containing peptides are evident. In one, the peptide masses are

dx.doi.org/10.1021/bi400963j | *Biochemistry* 2013, 52, 7271−7282

Table 1. Monoisotopic ($M + H^+$) Masses of Selected Ions from Tryptic Digests of *Bp*KatG before and after PAA Treatment

W, M, Y and C	SEQUENCE	Expected	Observed Control	Observed + PAA	%
W42, W43	DWWPNQLDSILHR	1792.91	1792.92	1792.89	
W94, W95	DLHALMTTSQDWWPADFGHYGGLFIR	3034.43	3034.46	nd	
W111	MAWHSAGTYR	1179.54	Nd	nd	
W139	FAPLNSWPDNANLDK	1701.82	1701.82	1701.83 1717.82 1733.82	40 18 42 (on W139 by MSMS)
W153	LLWPIK	769.50	769.50	769.49 801.49	46 54
W165, M180	AISWADLLILTGNVALESMGFK	2349.25	2349.26	2365.26	100 (on M180 by MSMS)
W195, W202	ADTWEPEDVYWGSEK	1811.78	1811.78	1811.79	
W208	IWLELSGGPNSR	1328.70	1328.69	1328.69	
W309	THGAGPASNVGAEPEAAG-IEAQGLGWK	2575.25	2575.27	nd	
W330, W337, W350	GADAITSGLEVTWTTTPQWSHNFFENLFGYEWELTK	4277.01	4277.05	nd	
W362	SPAGAHQWVAK	1151.60	1151.60	1151.58	
W446	YLGPEVPAEVLLWQDPIPAVDHPLIDAADAAELK	3665.91	3665.93	3665.91 3697.93	59 41 MSMS
W485	VLASGLTVSQLVSTAWAAASTFR	2336.26	2336.26	nd	
W513	DWEANQPEQLAAVLETLEAIR	2396.21	2396.21	2396.22	81
				2428.22	19
W513	LAPQKDWEANQPEQLAAVLETLEAIR	2933.54	2933.55	2933.55	
M671, W675	EQALTNDFFVNLLDMGTEWKPTAADADVFEGR	3600.70	3600.71	3600.70 3616.71 3632.72 3648.73	24 42 (on M671 by MSMS) 18 16
W697	WTGTRVDLVFGSHSQLR	1959.02	1959.01	nd	
W736	DFVAVWNK	978.51	978.51	978.50	
M264, M266	MAMNDEETVALIAGGHTFGK	2091.98	2091.96	2123.99	100 (M264 and/or M266 by MSMS)
M385	HRPTMLTTCLSLR	1540.83	1540.83	1540.83 1556.83	16 84
M591	ADASQEQTDVESMAVLEPVADGFR	2565.18	2565.19	2565.18 2581.19	17 83 (on M591 by MSMS[b])
M631	AQLLTLSAPEMTVLLGGLR	1983.13	1983.13	1983.14 1999.13	25 75 (on M631 by MSMS)
M740	VMNLDRFDLA	1193.60	1193.60	1193.60 1209.60	55 45
W111-Y238	QLENPLAAVQMGLIYVNPEGPDGNPDPVAAAR | MAWHSAGTYR	4493.18 4509.18 4525.18 4541.18	tr tr 4525.13 (M) 4540.21 (M)	nd nd nd nd	

dx.doi.org/10.1021/bi400963j | *Biochemistry* 2013, 52, 7271−7282

Table 1. continued

W, M, Y and C	SEQUENCE	Expected	Observed Control	Observed + PAA	%
W111-Y238-M264	MAMNDEETVALIAGGHTFGK | QLENPLAAVQMGLIYVNPEGPDGNPDPVAAAR | MAWHSAGTYR	6583.17	6585	nd	
C27	CPFHQAAGNGTSNR	1459.65	1459.66 (minor)		
C27-C27	CPFHQAAGNGTSNR | CPFHQAAGNGTSNR	2916.30	2933.51	2933.51	Location of extra OH nd
C556	QVSLADLIVLAGCAGVEQAAK	2056.11	2056.10	2104.08	100% 3O on C556 by MSMS

[a]nd, not detected. [b]MSMS sequencing suggests a modification best explained by a postoxidation cyclization involving the adjacent Ser590.

increased by 16, 32, or 48 Da, consistent with the addition of one, two, or three oxygen atoms, respectively, and in the second, the peptides could not be found in the spectrum. For example, the peptides containing W_{139}, W_{153}, W_{446}, and W_{513} are increased by 16 or 32 Da, whereas the peptides containing W_{94} + W_{95}, W_{111}, W_{309}, W_{330} + W_{337} + W_{350}, W_{485}, and W_{697} could not be identified in the spectrum after PAA treatment. The absence of a peptide in the spectrum is assumed to imply its modification although the form of modification or fate of the peptides could not be determined. Beyond the simple addition of oxygen atoms to the indole ring, a variety of more extensive oxidative modifications involving indole ring cleavage and rearrangement have been reported[35,36] and such a multiplicity of products would explain the failure to identify some of the peptides.

Similarly, the masses of peptides containing M_{180}, M_{385}, M_{631}, M_{591}, M_{671}, and M_{740} are increased by 16 and 32 Da. The location of oxidation on some of the more abundant peptides was confirmed by MS-MS sequencing (Table 1). Many of the modified or absent residues are either within 15 Å of the heme iron (for example, W_{139}, W_{153}, W_{330}, M_{264}, M_{180}, and M_{385}, measuring from the indole-N or S) consistent with facile electron migration to the heme. Of those residues further away, methionines close to the surface of the protein and accessible to PAA (for example, M_{671} and M_{740}) may react directly. However, very few surface accessible tryptophan residues suffered PAA oxidation (for example, W_{446} and W_{513} but not W_{42}, W_{43}, W_{195}, W_{202}, W_{208}, or W_{362}) suggesting that most modified tryptophans (indole oxides) are the products of initial internal electron transfer events followed by reaction of the indole radical with water or oxygen. Of the two cysteine-containing peptides, the surface-accessible C_{556}-containing peptide is increased in mass by 48 Da suggesting its conversion to cysteic acid. The peptide containing C_{27} is present in the native or untreated protein predominantly as a C_{27}−C_{27} cross-linked peptide (albeit 17 Da larger than expected suggesting the presence of an OH group), and this mass did not change as a result of PAA treatment. Surprisingly, no evidence for tyrosine oxidation was found.

The cross-linked M_{264}−Y_{238}−W_{111} adduct contains two easily oxidized residues and was of special interest because it is essential for catalase activity in KatGs. As we have reported previously,[37] even in the control or untreated sample, some cleavage of the adduct is detected, which must occur during either trypsin digestion or ionization because the crystal structure of the same sample of protein contains a 100% intact adduct. Despite this complication, the mass spectrum includes easily identified ions corresponding to the complete M−Y−W (6585 Da) adduct and the cleavage products Y−W (4493−4540 Da) and M_{264}-containing peptide (2092 Da). Following PAA treatment, both the 6585 Da M−Y−W and 4493−4540 Da Y−W composite peptides disappear from the spectrum and are not replaced by new peptides that can be identified. The 2092 Da M_{264}-containing peptide (M_{264}AMNDEETVALIAGGHTFGK) is replaced by a 2124 Da ion, consistent with the addition of two oxygen atoms. Unfortunately, because both methionines are at one end of the peptide, MS-MS sequencing could not differentiate between there being one oxygen atom on each methionine or both on one. While the fate of the Y−W component is not clear, its disappearance along with complete oxidation of the M_{264} peptide is consistent with disruption of the adduct.

PAA-Mediated Subunit Cross-Linking in KatGs. It has been reported that treatment of *Mt*KatG with *t*BHP causes cross-linking of the subunits to a predominantly dimeric form.[16] In light of the broad scope of oxidation caused by PAA at room temperature, its effect on possible cross-linking was investigated for similar outcomes. Consistent with the earlier reports of disulfide bonds in *Mt*KatG [38] and a fungal KatG [39] and with the Cys_{27}−Cys_{27} linkage observed in mass spectra, both *Bp*KatG and *Mt*KatG are predominantly in cross-linked, dimeric form (Figure 6, lanes a and g) that is largely but not completely sensitive to reducing agents (Figure 6, lanes b and h). Approximately 15% of residual dimeric protein remains after β-mercaptoethanol treatment suggestive of non-disulfide cross-linking.

Treatment of *Bp*KatG with a 500-fold excess of *t*BHP or a 1000-fold excess of H_2O_2 at 25 °C for 10 min (Figure 6, lanes e and f, respectively) causes little or no change in the protein pattern. Similarly, treatment with a 100-fold excess of PAA at 0 °C for 30 s causes little change (Figure 6, lane c). However, treatment with the same 100-fold excess of PAA at 25 °C for 10 min causes a dramatic shift of almost all of the monomer and dimer forms into a mixture of very large multimeric forms

dx.doi.org/10.1021/bi400963j | *Biochemistry* 2013, 52, 7271−7282

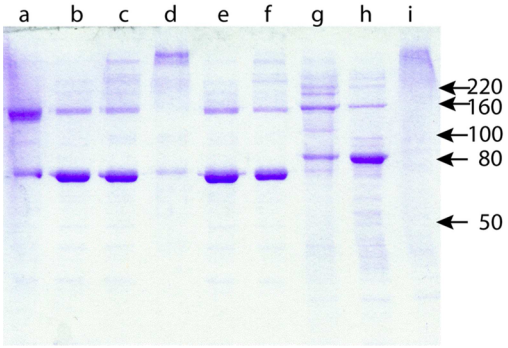

Figure 6. SDS denaturing gel of 0.012 mM *Bp*KatG and *Mt*KatG treated under various conditions. Lanes a and g: untreated *Bp*KatG or *Mt*KatG, respectively, denatured in the absence of reducing agent. Samples in all other lanes were denatured in the presence of 10 mM *β*-mercaptoethanol. Lane b: untreated *Bp*KatG. Lane c: *Bp*KatG treated with 1 mM PAA for 30 s at 0 °C. Lane d: *Bp*KatG treated with 1 mM PAA for 10 min at 25 °C. Lane e: *Bp*KatG treated with 5 mM *t*BHP for 10 min at 25 °C. Lane f: *Bp*KatG treated with 10 mM H_2O_2 for 10 min at 25 °C. Lane h: untreated *Mt*KatG. Lane i: *Mt*KatG treated with 1 mM PAA for 10 min at 25 °C.

(Figure 6, lane d). A similar treatment of *Mt*KatG causes an even more thorough conversion of monomer and dimer into a smear of much larger protein (Figure 6, lane i). Therefore, unlike the earlier report[16] that employed a longer incubation period with *t*BHP to generate non-disulfide linked dimers, an accumulation of multimeric species was observed here only with PAA.

Attempts to characterize the cross-linked mixture by electrospray ionization MS were not successful. The spectra confirm that the dimer and tetramer species decreased in intensity, but only a small amount of an octamer and larger forms were observed and only transiently. A loosely associated tetrameric KatG species has previously been reported for *Escherichia coli* KatG or HPI [40] and is not unexpected. Despite the spectrometer being capable of identifying multimers with up to 16 subunits, no larger material was present in sufficient abundance to be identified suggesting either very large multimers or a very broad range of sizes that diluted out individual ions. Attempts to identify cross-linked peptides in tryptic digests by MS-MS were also unsuccessful, consistent with the formation of a variety of cross-links, none in sufficient amounts to be identified. The unique sensitivity of KatGs to PAA modification is evident in there being no change in the multimeric size in horseradish peroxidase, bovine liver catalase, or *E. coli* catalase KatE after similar treatment (data not shown). This is not the first demonstration of oxidative cross-linking in KatGs,[16,41] but it is the first to recognize its extent.

Inhibition of the Catalatic and Peroxidatic Reactions by PAA. It was anticipated that such extensive damage to the M−Y−W adduct and modification of the peroxidatically important W_{139} and W_{153} would affect the catalatic and peroxidatic activities. This was confirmed in direct assays wherein preincubation of *Bp*KatG with a 50-fold excess of PAA caused a time-dependent reduction in both the catalatic (Figure 7a, solid lines) and peroxidatic (Figure 7a, dashed lines) reactions. A comparison of activities following 15 min preincubation at 20 °C reveals slightly more inhibition by *m*CPBA than PAA, whereas a 2500-fold excess of *t*BHP or the mixture of glucose and glucose oxidase had no effect (Table 2). Even a 10-fold excess of PAA caused inhibition, albeit more

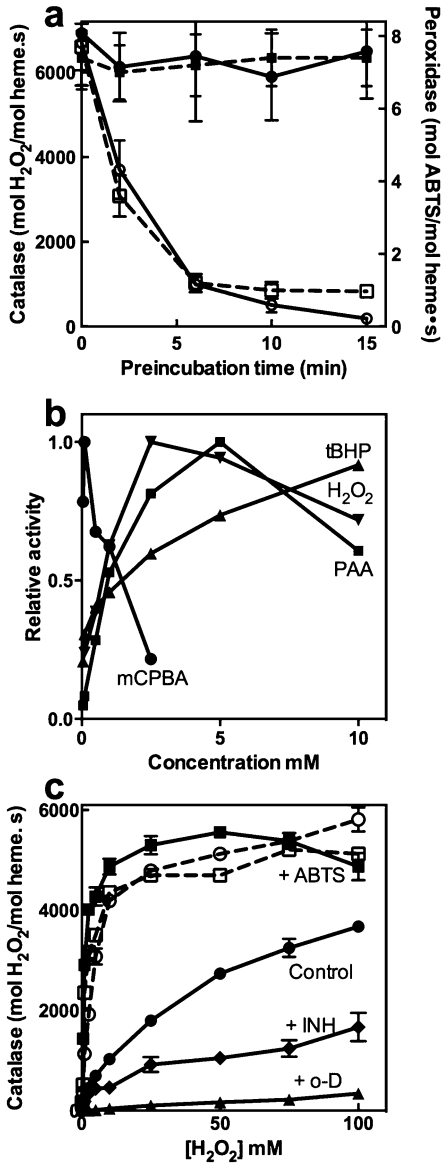

Figure 7. (a) Inhibition of catalatic and peroxidatic reactions by preincubation with PAA. Catalase activity was determined at pH 7 and 37 °C after preincubation at 20 °C for the times shown with water (solid line, ●) or 0.5 mM PAA (solid line, ○). Peroxidase activity was determined at pH 5 and 25 °C after preincubation at 20 °C for the times shown with water (dashed line, ■) or 0.5 mM PAA (dashed line, □). (b) Relative peroxidatic activity as a function of oxidant concentration. The rates are normalized to the maximum rate shown in Table 3 for comparison: H_2O_2 (▼), PAA (■), *t*BHP (▲), and *m*CPBA (●). (c) Effect of peroxidatic substrates on the catalatic reaction as a function of H_2O_2 concentration at pH 7 (dashed lines) and pH 5 (solid lines). Included in the various reactions were water as control (○,●), 5 mM ABTS (□,■), 1 mM INH (◆), and 0.5 mM o-dianisidine (▲). The activation by ABTS at low H_2O_2 concentration is evident only at pH 5 (solid lines) and is to the same level as the maximum rate at pH 7.

slowly. The peroxidatic substrate ABTS provided some protection against PAA inhibition, more when added before PAA than after. Dialysis of the protein following prolonged treatment with PAA did not reverse the loss of activity, consistent with the irreversible oxidative damage observed by MS.

dx.doi.org/10.1021/bi400963j | *Biochemistry* 2013, 52, 7271−7282

Table 2. Effect of Preincubation with Various Oxidants and Peroxidatic Substrates on the Catalatic and Peroxidatic Activities of *Bp*KatG

addition[a]	rate[a]	
	catalase[b]	peroxidase[c]
control	5130 ± 320	6.4 ± 0.90
+ 0.1 mM PAA	250 ± 21	5.1 ± 0.60
+ 0.5 mM PAA	83 ± 1	2.1 ± 0.09
+ 0.5 mM *m*CPBA	14.6 ± 6	1.0 ± 0.01
+ 25 mM *t*BHP	5130 ± 360	6.6 ± 0.86
+ GOX + glucose	5510 ± 370	6.5 ± 1.5
+ 1 mM ABTS	5590 ± 650	5.9 ± 0.23
+ 0.5 mM PAA + 1 mM ABTS	410 ± 68	2.6 ± 0.42
+ 1 mM ABTS then 0.5 mM PAA	1965 ± 240	3.5 ± 0.31

[a]Catalase activity is expressed as μmol H_2O_2 converted to $O_2 \cdot s^{-1} \cdot (\mu mol\ heme)^{-1}$. Peroxidase activity was determined using ABTS (ε_{405} = 36 800 M^{-1} cm^{-1}) as electron donor, and the rate is expressed as μmol ABTS oxidized$\cdot s^{-1} \cdot (\mu mol\ heme)^{-1}$. [b]*Bp*KatG (10 μM) was incubated for 15 min with the different components before addition to the catalase reaction assay in 50 mM potassium phosphate, pH 7, with 60 mM H_2O_2 at 37 °C. Similar values were determined at pH 5 in 50 mM sodium acetate with 120 mM H_2O_2 at 37 °C. [c]*Bp*KatG (10 μM) was incubated for 15 min with the different components before addition to the peroxidase reaction assay in a solution of 0.4 mM ABTS at pH 5.0 and 25 °C with 2.5 mM H_2O_2.

Table 3. Variation in Peroxidatic Reaction Rate of KatGs as a Function of Oxidant[a]

oxidant	rate[b]
A. *Bp*KatG	
2.5 mM H_2O_2	6.4 ± 0.9
5.0 mM PAA	102.0 ± 11.2
25 mM *t*BHP	7.2 ± 0.9
0.1 mM *m*CPBA	37.0 ± 3.3
GOX + glucose	3.5 ± 0.3
B. *Mt*KatG	
2.5 mM H_2O_2	10.0 ± 2.5[2]
25 mM *t*BHP	5.4 ± 1.1

[a]The peroxidase assay was carried out in 50 mM sodium acetate, pH 5.0, with 0.4 mM ABTS at 25 °C. Rates were corrected for any reaction occurring in the absence of enzyme. [b]The rate is expressed as μmol ABTS oxidized$\cdot s^{-1} \cdot (\mu mol\ heme)^{-1}$.

In light of the detrimental effects of PAA on catalytic function and internal protein modification, its effectiveness in supporting the peroxidatic reaction was also reviewed in comparison to other commonly used oxidants (Table 3). Both PAA and *m*CPBA support higher peroxidatic rates than H_2O_2 or *t*BHP, reaching a maximum at 5 and 0.1 mM, respectively, and then dropping at higher concentrations (Figure 7b). It should be noted that the *t*BHP-dependent peroxidatic rates of *Mt*KatG and *Bp*KatG are similar (Table 3) and are significantly higher (100-fold) than reported previously,[9] at least in part because those assays were carried out at pH 7.5 rather than the optimum pH 5.0.[2,42] The drop in peroxidatic rate at higher concentrations of PAA is most likely associated with oxidative damage, whereas the drop in rate at concentrations of H_2O_2 above 2.5 mM arises from competition with the catalatic reaction, which is still much faster than the peroxidatic reaction despite the increase in K_M from 5 to 60 mM between pH 5 and 7. [2] Competition as well as synergy between the catalatic and peroxidatic processes is also evident in the wide variation in effects of different peroxidatic electron donors on the catalatic process ranging from moderate to strong inhibition by INH (Figure 7c) and o-dianisidine,[20] respectively, to activation by ABTS.[43] In fact, ABTS activation is evident only at pH 5 (Figure 7c, solid line) and the maximum catalatic turnover rate in the presence of 5 mM ABTS never exceeds the maximum rate achieved at pH 7 (Figure 7c, dashed line). Increasing ABTS above 5 mM causes an increasing inhibition of the catalatic process similar to other peroxidatic substrates (not shown).

DISCUSSION

The functional complexity of KatGs, which combine significant catalatic and peroxidatic capabilities with the slower reactions of INH cleavage, superoxide formation, and isonicotinyl-NAD synthesis has presented many challenges but at the same time has provided a unique opportunity to understand better the interdependencies of the reaction mechanisms in multifunctional heme enzymes. The heme-containing core of the enzyme is the reaction center for the catalatic and peroxidatic reactions as well as for superoxide formation, but the binding site(s) for electron donors (or substrates) required for the reduction of high-valent ferryl-oxo intermediates (peroxidase reaction) and molecular oxygen (superoxide formation) remains poorly defined with only one INH binding site having been characterized, and it is remote from the heme cavity.[6]

One seeming peculiarity of KatGs is the unusually high tryptophan content, 23 per monomer in *Bp*KatG of which 17 are in the catalytically active 420 residue N-terminal domain. One obvious role for tryptophan residues is in electron transfer between substrates and the heme, and this has been confirmed in the identification of three tryptophan-based high-valent ferryl intermediates in the peroxidase cycle of *Bp*KatG, with W_{330}, W_{139}, and W_{153} as the radical sites and W_{111}, W_{94}, and W_{95} having a crucial role in facilitating long-range electron transfer.[11] However, electron transfer also occurs in CCP, which has one tryptophan radical site (W_{191}) out of the six tryptophans in 294 residues leaving open the question of why there are so many tryptophans in KatGs. The extensive oxidative modification of tryptophan, methionine, and cysteine residues caused by PAA provides a clue.

In this work, we show that the same [Fe^{IV}=O $W_{330}^{\bullet+}$], [Fe^{IV}=O $W_{139}^{\bullet}$], and [Fe^{IV}=O $W_{153}^{\bullet}$] intermediates are formed by the reaction of *Bp*KatG with either low (10-fold) or much higher (1000-fold) excesses of PAA. However, the higher concentration of PAA causes a much more rapid loss of the tryptophan- and tyrosine-based radical intermediates coincident with the conversion to a persistent [Fe^{IV}=O] intermediate. It is also significant that the high excess of PAA induced the formation of a new radical species, tentatively assigned to a sulfur-based radical and possibly explained by the cleavage of the M−Y−W adduct creating a radical on M_{264} prior to its oxidation evident in the M_{264}-containing peptide.

The reduction of PAA by *Bp*KatG occurs via two general routes. In the first, PAA oxidizes the heme to ferryl intermediates, which are then reduced by electrons drawn from various residues in the protein. Because no peroxidatic electron donors are present, the resulting protein radicals eventually react with water or oxygen to produce the modified peptides identified in the mass spectrum. This effectively establishes a modified peroxidatic cycle with repeated cycles of heme oxidation by PAA and ferryl reduction utilizing electrons from internal tryptophan and methionine residues. However,

dx.doi.org/10.1021/bi400963j | *Biochemistry* 2013, 52, 7271−7282

the number of rounds in this cycle is limited by the number of residues that can donate electrons, because each residue can participate only once before being terminally modified. As the availability of electron-donating residues diminishes and the [Fe^{IV}=O] species accumulates, the peroxidatic activity decreases. Not surprisingly, W_{139} and W_{153}, both sites of stable radical accumulation in the peroxidatic process, are among the modified amino acids, providing another explanation for the loss of peroxidatic activity. The EPR evidence for a radical tentatively assigned to a sulfur-based radical obtained in the conditions of 1000-fold excess PAA suggests that some internal methionine residues may also supply electrons for such a cycle, although cleavage of the M−Y−W adduct may equally well explain the radical. The second general route involves the direct reaction with PAA of other methionines and the single cysteine residue, particularly those that are surface accessible. Somewhat surprising in light of the prevalence of Tyr-based radicals in *Bp*KatG and a report of dityrosine formation[44] is the absence of detected modification on any tyrosine-containing peptides. The topic of protein oxidative modification under various ionizing conditions has been reviewed.[45]

The obvious advantage to KatGs of having a multiplicity of sites that are sensitive to oxidation is that it provides a finite level of antioxidant protection to an enzyme that itself has an antioxidant function and is therefore in contact with oxidizing species. A previous example of such intraprotein protection being imparted by methionine oxidation in glutamine synthetase has been documented.[46] Enhancing the importance of methionine oxidation is the existence of methionine sulfoxide reductases,[47] which *in vivo* regenerate the surface situated methionines allowing their repeated use as endogenous antioxidant sites. In fact, it is unlikely that the internally oxidized methionines would be repaired in KatGs and a tryptophan oxide reductase has not been reported, making the inactivation of *Bp*KatG inevitable in the presence of high oxidant levels.

In conclusion, we have shown that in the absence of endogenous electron-donor substrates, *Bp*KatG can react with low excesses of PAA and return to the resting state still catalytically active. However, prolonged incubation of KatGs with PAA or exposure to high excesses of PAA cause inactivation of both the catalatic and peroxidatic reactions. The same high-valent ferryl-oxo intermediates are formed with both low and high excesses of PAA, but the high excess promotes a more rapid conversion of the protein-based radical intermediates to a [Fe^{IV}=O] species. PAA is reduced either through direct oxidation of surface-located methionine and cysteine residues or through a modified peroxidatic cycle wherein the protein radical intermediates, including those on W_{139} and W_{153}, are ultimately quenched in a reaction with water or molecular oxygen. The modified residues are inactive for further electron donation leading to inhibition of the peroxidatic reaction. Disruption of the M−Y−W adduct causes inhibition of the catalatic reaction. The two subunits of wild-type *Bp*KatG are predominantly joined by a cysteine−cysteine link in the native state, but PAA causes additional non-cysteine cross-linking of subunits into very large multimeric structures.

AUTHOR INFORMATION

Corresponding Author

*E-mail: Peter.Loewen@umanitoba.ca. Phone: 204 797 2134. Fax: 204 474 7603.

Funding

This work was supported by a Discovery Grant 9600 from the Natural Sciences and Engineering Research Council (NSERC) of Canada (to P.C.L.), the Canada Research Chair Program (to P.C.L.), the French CNRS and CEA-Saclay (UMR 8221) (to A.I.), and the CNRS Program PICS-Canada #05865 (to A.I.).

Notes

The authors declare no competing financial interest.

ACKNOWLEDGMENTS

We thank V. Spicer and V. Collado for technical assistance and K. Standing and W. Ens for continued unrestricted access to the instruments in the Time-of-Flight Laboratory, Dept. of Physics and Astronomy, University of Manitoba.

ABBREVIATIONS

EPR, electron paramagnetic resonance; ABTS, 2,2′-azinobis(3-ethylbenzothiazolinesulfonic acid); *t*BHP, *t*-butyl hydroperoxide; *m*CPBA, *m*-chloroperoxybenzoic acid; PAA, peroxyacetic acid; KatG, catalase-peroxidase; *Bp*KatG, *Burkholderia pseudomallei* KatG; *Mt*KatG, *Mycobacterium tuberculosis* KatG; GOX, glucose oxidase; MS, mass spectrometry; CT, charge transfer; INH, isonicotinic acid hydrazide or isoniazid

REFERENCES

(1) Dunford, H. B. (1999) *Heme Peroxidases*, Wiley-VCH, Toronto
(2) Singh, R., Wiseman, B., Deemagarn, T., Jha, V., Switala, J., and Loewen, P. C. (2008) Comparative study of catalase-peroxidases (KatGs). *Arch. Biochem. Biophys. 471*, 207−214.
(3) Switala, J., and Loewen, P. C. (2002) Diversity of properties among catalases. *Arch. Biochem. Biophys. 401*, 145−154.
(4) Hillar, A., and Loewen, P. C. (1995) Comparison of isoniazid oxidation catalyzed by bacterial catalase-peroxidases and horseradish peroxidase. *Arch. Biochem. Biophys. 323*, 438−446.
(5) Carpena, X., Wiseman, B., Deemagarn, T., Singh, R., Switala, J., Ivancich, A., Fita, I., and Loewen, P. C. (2005) A molecular switch and electronic circuit modulate catalase activity in catalase-peroxidases. *EMBO Rep. 6*, 1156−1162.
(6) Wiseman, B., Carpena, X., Feliz, M., Donald, L. J., Pons, M., Fita, I., and Loewen, P. C. (2010) Isonicotinic acid hydrazide conversion to isonicotinyl-NAD by catalase-peroxidases. *J. Biol. Chem. 285*, 26662−26673.
(7) Wengenack, N. L., Hoard, H. M., and Rusnak, F. (1999) Isoniazid oxidation by *Mycobacterium tuberculosis* KatG: A role for superoxide which correlates with isoniazid susceptibility. *J. Am. Chem. Soc. 121*, 9748−9749.
(8) Singh, R., Wiseman, B., Deemagarn, T., Donald, L. J., Duckworth, H. W., Carpena, X., Fita, I., and Loewen, P. C. (2004) Catalase-peroxidases (KatG) exhibit NADH oxidase activity. *J. Biol. Chem. 279*, 43098−43106.
(9) Cade, C. E., Dlouhy, A. C., Medzihradszky, K. F., Salas-Castillo, S. P., and Ghiladi, R. A. (2010) Isoniazid-resistance conferring mutations in *Mycobacterium tuberculosis* KatG: catalase, peroxidase and INH-NADH adduct formation activities. *Protein Sci. 19*, 458−474.
(10) Zhao, X., Yu, S., Wang, F., Sacchettini, J. C., and Magliozzo, R. S. (2006) Hydrogen peroxide-mediated isoniazid activation catalyzed by *Mycobacterium tuberculosis* catalase-peroxidase (KatG) and its S315T mutant. *Biochemistry 45*, 4131−4140.
(11) Colin, J., Wiseman, B., Switala, J., Loewen, P. C., and Ivancich, A. (2009) Distinct role of specific tryptophans in facilitating electron transfer or as [Fe(IV)=O $Trp^{\bullet}$] intermediates in the peroxidase reaction of *Burkholderia pseudomallei* catalase-peroxidase: a multi-frequency EPR spectroscopy investigation. *J. Am. Chem. Soc. 131*, 8557−8563.

(12) Couchane, S., Lippai, I., and Magliozzo, R. S. (2000) Catalase-peroxidase (*Mycobacterium tuberculosis* KatG) catalysis and isoniazid activation. *Biochemistry 39*, 9975−9983.
(13) Wiseman, B., Colin, J., Smith, A. T., Ivancich, A., and Loewen, P. C. (2009) Mechanistic insight into the initiation step of the reaction of *Burkholderia pseudomallei* catalase-peroxidase with peroxyacetic acid. *J. Biol. Inorg. Chem. 14*, 801−811.
(14) Ghiladi, R. A., Cabelli, D. E., and Ortiz de Montellano, P. R. (2004) Superoxide reactivity of KatG: Insights into isoniazid resistance pathways in TB. *J. Am. Chem. Soc. 126*, 4772−4773.
(15) Ghiladi, R. A., Medsihradszky, K. F., Rusnak, F. M., and Ortiz de Montellano, P. M. (2005) Correlation between isoniazid resistance and superoxide reactivity in *Mycobacterium tuberculosis* KatG. *J. Am. Chem. Soc. 127*, 13428−13442.
(16) Ranguelova, K., Suarez, J., Magliozzo, R. S., and Mason, R. P. (2008) Spin trapping investigation of peroxide- and isoniazid-induced radicals in *Mycobacterium tuberculosis* catalase-peroxidase. *Biochemistry 47*, 11377−11385.
(17) Gumiero, A., Murphy, E. J., Metcalfe, C. L., Moody, P. C. E., and Raven, E. L. (2010) An analysis of substrate binding interactions in the heme peroxidase enzymes: a structural perspective. *Arch. Biochem. Biophys. 500*, 13−20.
(18) Fielding, A. J., Singh, R., Boscolo, B., Loewen, P. C., Ghibaudi, E. M., and Ivancich, A. (2008) Intramolecular electron transfer versus substrate oxidation in lactoperoxidase: Investigation of radical intermediates by stopped-flow absorption spectrophotometry and (9−285 GHz) Electron Paramagnetic Resonance Spectroscopy. *Biochemistry 47*, 9781−9792.
(19) Singh, R., Switala, J., Loewen, P. C., and Ivancich, A. (2007) Two [Fe(IV)=O Trp$^{\bullet}$] intermediates in *M. tuberculosis* catalase-peroxidase discriminated by multifrequency (9−285 GHz) EPR spectroscopy: reactivity toward isoniazid. *J. Am. Chem. Soc. 129*, 15954−15963.
(20) Claiborne, A., and Fridovich, I. (1979) Purification of the o-dianisidine peroxidase from *Escherichia coli* B: physicochemical characterization and analysis of its dual catalatic and peroxidatic activities. *J. Biol. Chem. 254*, 4245−4252.
(21) Regelsberger, G., Jakopitsch, C., Engleder, M., Rüker, F., Peschek, G. A., and Obinger, C. (1999) Spectral and kinetic studies of the oxidation of monosubstituted phenols and anilines by recombinant *Synechocystis* catalase-peroxidase compound I. *Biochemistry 38*, 10480−10488.
(22) Collins, D. P., Isaac, I. S., Coulter, E. D., Hager, P. W., Ballou, D. P., and Dawson, J. H. (2012) Reaction of ferric *Caldariomyces fumago* chloroperoxidase with *meta*-chloroperoxybenzoic acid: Sequential formation of compound I, compound II and regeneration of the ferric state using one reactant. *J. Porphyrins Phthalocyanines 16*, 1−10.
(23) Loewen, P. C., Switala, J., Smolenski, M., and Triggs-Raine, B. L. (1990) Molecular characterization of three mutations in *katG* affecting the activity of hydroperoxidase I of *Escherichia coli*. *Biochem. Cell Biol. 68*, 1037−1044.
(24) Hillar, A., and Loewen, P. C. (1995) Comparison of isoniazid oxidation catalyzed by bacterial catalase-peroxidases and horseradish peroxidase. *Arch. Biochem. Biophys. 323*, 438−446.
(25) Carpena, X., Switala, J., Loprasert, S., Mongkolsuk, S., Fita, I., and Loewen, P. C. (2002) Crystallization and preliminary X-ray analysis of the catalase-peroxidase KatG from *Burkholderia pseudomallei*. *Acta Crystallogr. D58*, 3184−2186.
(26) Rorth, M., and Jensen, P. K. (1967) Determination of catalase activity by means of the Clark oxygen electrode. *Biochim. Biophys. Acta 139*, 171−173.
(27) Childs, R. E., and Bardsley, W. G. (1975) The steady-state kinetics of peroxidase with 2, 2′-azino-di-(3-ethylbenthiazoline-6-sulphonic acid) as chromogen. *Biochem. J. 145*, 93−103.
(28) Layne, E. (1957) Spectrophotometric and turbidimetric methods for measuring proteins. *Methods Enzymol. 3*, 447−454.
(29) Laemmli, U. K. (1970) Cleavage of structural proteins during the assembly of the head of bacteriophage T4. *Nature 227*, 680−685.
(30) Weber, K., Pringle, J. R., and Osborn, M. (1972) Measurement of molecular weights by electrophoresis on SDS-acrylamide gels. *Methods Enzymol. 26*, 3−27.
(31) Shevchenko, A., Loboda, A., Shevchenko, A., Ens, W., and Standing, K. G. (2000) MALDI quadrupole time-of-flight mass spectrometry: A powerful tool for proteomic research. *Anal. Chem. 72*, 2132−2141.
(32) Loboda, A. V., Krutchinsky, A. N., Bromirski, M., Ens, W., and Standing, K. G. (2000) A tandem quadrupole/time-of-flight mass spectrometer with a matrix-assisted laser desorption/ionization source: design and performance. *Rapid Commun. Mass Spectrom. 14*, 1047−1057.
(33) Kozlovski, V. I., Donald, L. J., Collado, V. M., Spicer, V., Loboda, A. V., Chernushevich, I. V., Ens, W., and Standing, K. G. (2011) A TOF mass spectrometer for the study of noncovalent complexes. *Int. J. Mass Spectrom. 308*, 118−125.
(34) Carpena, X., Wiseman, B., Deemagarn, T., Herguedas, B., Ivancich, A., Singh, R., Loewen, P. C., and Fita, I. (2006) Roles for Arg426 and Trp111 in the modulation of NADH oxidase activity of the catalase-peroxidase KatG from *Burkholderia pseudomallei* inferred from pH-induced structural changes. *Biochemistry 45*, 5171−5179.
(35) Perdivara, I., Deterding, L. J., Przybylski, M., and Tomer, K. B. (2010) Mass spectrometric identification of oxidative modifications to tryptophan residues in proteins: chemical artifact or post-translational modification? *J. Am. Soc. Mass Spectrom. 21*, 1114−1117.
(36) Gracanin, M., Hawkins, C. L., Pattison, D. I., and Davies, M. J. (2009) Singlet-oxygen-mediated amino acid and protein oxidation: formation of tryptophan peroxides and decomposition products. *Free Radical Biol. Med. 47*, 92−102.
(37) Donald, L. J., Krokhin, O. V., Duckworth, H. W., Wiseman, B., Deemagarn, T., Singh, R., Switala, J., Carpena, X., Fita, I., and Loewen, P. C. (2003) Characterization of the catalase-peroxidase KatG from *Burkholderia pseudomallei* by mass spectrometry. *J. Biol. Chem. 278*, 35687−35692.
(38) Saint-Joanis, B., Souchon, H., Wilming, M., Johnsson, K., Alzari, P. M., and Cole, S. T. (1999) Use of site-directed mutagenesis to probe the structure, function and isoniazid activation of the catalase/peroxidase, KatG, from *Mycobacterium tuberculosis*. *Biochem. J. 338*, 753−760.
(39) Zamocky, M., Garcia-Fernández, Q., Gasselhuber, B., Jakopitsch, C., Furtmüller, P. G., Loewen, P. C., Fita, I., Obinger, C., and Carpena, X. (2012) High conformation stability of secreted eukaryotic catalase-peroxidases - answers from the first crystal and unfolding studies. *J. Biol. Chem. 287*, 32254−32262.
(40) Loewen, P. C., and Switala, J. (1986) Purification and characterization of catalase HPII from *Escherichia coli* K12. *Can. J. Biochem. Cell Biol. 64*, 638−646.
(41) Zhao, X., Khajo, A., Jarrett, S., Suarez, J., Levitsky, Y., Burger, R. M., Jarzecki, A. A., and Magliozzo, R. S. (2012) Specific function of the Met-Tyr-Trp adduct radical and residues Arg-418 and Asp-137 in the atypical catalase reaction of catalase-peroxidase KatG. *J. Biol. Chem. 287*, 37057−37065.
(42) Johnsson, K., Froland, W. A., and Schultz, P. G. (1997) Overexpression, purification, and characterization of the catalase-peroxidase KatG from *Mycobacterium tuberculosis*. *J. Biol. Chem. 272*, 2834−2840.
(43) Ndontsa, E. N., Moore, R. L., and Goodwin, D. C. (2012) Stimulation of KatG catalase activity by peroxidatic electron donors. *Arch. Biochem. Biophys. 525*, 215−222.
(44) Lardinois, O. M., and Ortiz de Moltellano, P. R. (2001) H_2O_2-mediated crosslinking between lactoperoxidase and myoglobin. *J. Biol. Chem. 276*, 23186−23191.
(45) Stadtman, E. R. (1993) Oxidation of free amino acids and amino acid residues in proteins by radiolysis and by metal-catalyzed reactions. *Annu. Rev. Biochem. 62*, 797−821.
(46) Levine, R. L., Mosoni, L., Berlett, B. S., and Stadtman, E. R. (1996) Methionine residues as endogenous antioxidants in proteins. *Proc. Natl. Acad. Sci. U.S.A. 93*, 15036−15040.

(47) Brot, N., and Weissbach, H. (1983) Biochemistry and physiological role of methionine sulfoxide residues in proteins. *Arch. Biochem. Biophys. 223*, 271−281.